Biochimica et Biophysica Acta 1853 (2015) 549–560

Contents lists available at ScienceDirect

Biochimica et Biophysica Acta

journal homepage: www.elsevier.com/locate/bbamcr

Onconase induces autophagy sensitizing pancreatic cancer cells to gemcitabine and activates Akt/mTOR pathway in a ROS-dependent manner

Claudia Fiorini [a], Marco Cordani [a], Giovanni Gotte [a], Delia Picone [b], Massimo Donadelli [a,*]

[a] Department of Life and Reproduction Sciences, Biochemistry Section, University of Verona, Verona, Italy
[b] Department of Chemical Sciences, University of Naples "Federico II", Naples, Italy

ARTICLE INFO

Article history:
Received 21 October 2014
Received in revised form 5 December 2014
Accepted 11 December 2014
Available online 20 December 2014

Keywords:
autophagy
onconase
pancreatic cancer
reactive oxygen species (ROS)
mammalian target of rapamycin (mTOR)
gemcitabine

ABSTRACT

Onconase® (ONC) is a member of the RNase super-family that is secreted in oocytes and early embryos of *Rana pipiens*. Over the last years, research interest about this small and basic frog RNase, also called ranpirnase, constantly increased because of its high cytotoxicity and anticancer properties. Onconase is currently used in clinical trials for cancer therapy; however, the precise mechanisms determining cytotoxicity in cancer cells have not yet been fully investigated. In the present manuscript, we evaluate the antitumoral property of onconase in pancreatic adenocarcinoma cells and in non-tumorigenic cells as a control. We demonstrate that ONC stimulates a strong antiproliferative and proapoptotic effect in cancer cells by reporting for the first time that ONC triggers Beclin1-mediated autophagic cancer cell death. In addition, ONC inhibits the expression of mitochondrial uncoupling protein 2 (UCP2) and of manganese-dependent superoxide dismutase (MnSOD) triggering mitochondrial superoxide ion production. ONC-induced reactive oxygen species (ROS) are responsible for Akt/mTOR pathway stimulation determining the sensitivity of cancer cells to mTOR inhibitors and lessening autophagic stimulation. This indicates ROS/Akt/mTOR axis as a strategy adopted by cancer cells to reduce ONC-mediated cytotoxic autophagy stimulation. In addition, we demonstrate that ONC can sensitize pancreatic cancer cells to the standard chemotherapeutic agent gemcitabine allowing a reduction of drug concentration when used in combination settings, thus suggesting a lowering of chemotherapy-related side effects. Altogether, our results shed more light on the mechanisms lying at the basis of ONC antiproliferative effect in cancer cells and support its potential use to develop new anticancer strategies.

1. Introduction

Onconase (ONC, see Fig. 1A) is a highly cytotoxic member of the pancreatic-type ribonuclease (RNase) super-family [1] earlier named P-30 protein [2] but known as ranpirnase or onconase® (ONC, Alfacell Corporation, Somerset, NJ, USA). ONC is a monomer secreted in oocytes and early embryos of *Rana pipiens* and shares 30% sequence identity with the prototype RNase A even though it is smaller and more basic than the latter (104 residues versus 124, and pI 9.7 versus 9.3, respectively) [1–3]. ONC specifically evades the interaction with the cytosolic ribonuclease inhibitor (RI) owing to its particular structure which lacks the RNase A key-loop residues involved in the interaction with RI [4–6]. Such a capacity confers to ONC a high cytotoxic activity against several human cancer cell types, such as glioma cells [7] or lymphoma B cells [8]. Notably, ONC is currently used in Phase II and Phase IIIb clinical trials as therapy against non–small cell lung cancer and against unresectable malignant mesothelioma, respectively [9]. In addition to its anticancer properties, ONC is known to assume relevant roles as an anti-viral enzyme which inhibits HIV-1 virion production within viable replicating cells by degrading viral RNA and tRNALys [10,11].

Over the last years, autophagy has acquired an increasing relevance in cancer research [12]. It is a highly conserved cellular process in which cytoplasmic materials and organelles are sequestered into double-membrane autophagic vesicles called autophagosomes and delivered to lysosomes for degradation. This phenomenon occurs in response to environmental conditions or cellular stimuli, such as starvation [13], endoplasmic reticulum stress, and increased reactive oxygen species (ROS) [14,15]. Besides having a cytoprotective role in cellular homeostasis by acting as a cytoplasmic quality control mechanism which eliminates old or unfolded proteins and damaged organelles [16,17], autophagy can also be a form of programmed cell death, designated as "autophagic cell death" [18]. Then, the source of the lysosomal enzymes used for degradation of dying cells is one of the elements that distinguish apoptosis from autophagic cell death. The induction of several genes, including microtubule-associated protein 1 light chain 3 (LC3),

* Corresponding author at: Department of Life and Reproduction Sciences, Biochemistry Section, University of Verona, Strada Le Grazie 8, I-37134, Verona, Italy. Tel.: +39 045 8027281; fax: +39 045 8027170.
E-mail address: massimo.donadelli@univr.it (M. Donadelli).

http://dx.doi.org/10.1016/j.bbamcr.2014.12.016
0167-4889/

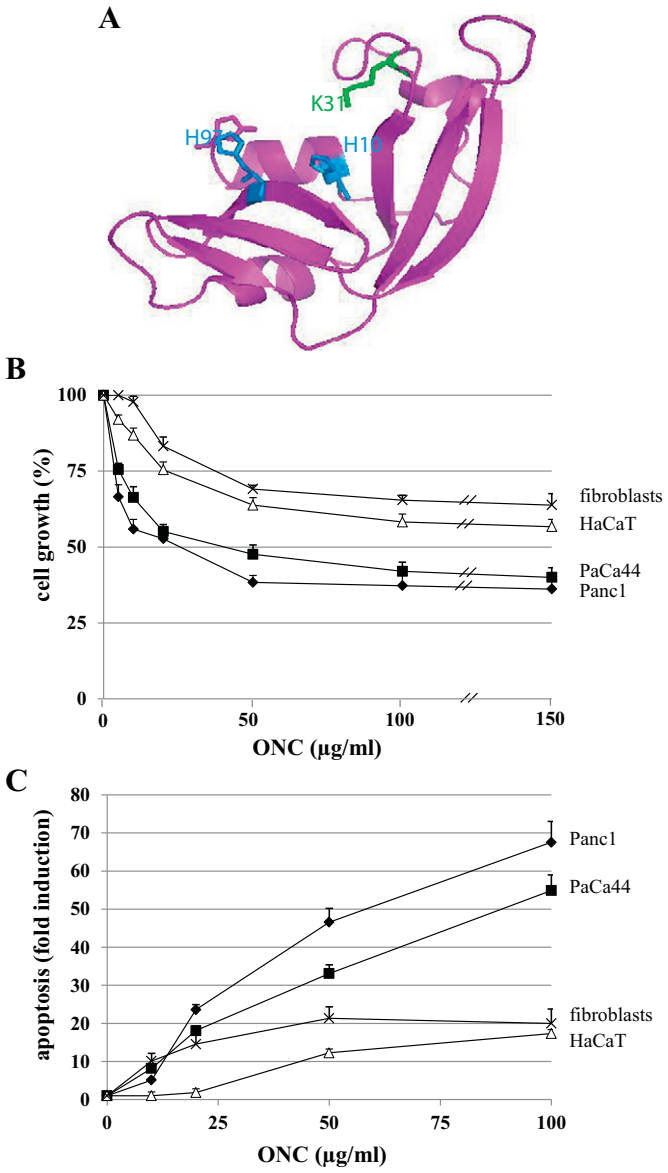

Fig. 1. Effect of ONC on growth inhibition and apoptosis in pancreatic cancer cell lines (Panc1 and PaCa44) and in non-tumoral cells (fibroblasts and HaCaT). (A) ONC structure (pdb code 1ONC): the residues of the catalytic triad are highlighted. (B) Cell growth determined with the crystal violet colorimetric assay. (C) Apoptosis analyzed using the annexin V/FITC binding assay. In both (B) and (C) panels, cells were seeded in 96-well plates, incubated overnight, and treated with increasing concentrations of onconase for 72 h. Values are means (±SD) of three independent biological replicates, each performed using three technical replicates (three wells).

Beclin1, and a number of autophagy-related genes (Atg) is required for the formation, maturation, and fusion of autophagic vesicles to lysosomes [19]. Furthermore, autophagy incorporates signaling through a different cellular pathway including the metabolic master regulators mammalian target of rapamycin (mTOR) and adenosine monophosphate-activated protein kinase (AMPK) [20].

Since the importance of the cytotoxic potential of some RNases belonging to the secretory pancreatic-type RNase super-family definitely increased in the last two decades, we investigated the effects of ONC on cells of human pancreatic adenocarcinoma, which is a particularly aggressive and devastating cancer type [21] characterized by chemoresistance to traditional therapeutic drugs including treatment with the gold standard nucleotide analogue gemcitabine (GEM; 2′,2′-difluoro-2′-deoxycytidine) [22,23]. In particular, we aimed to explore the link between autophagy, ROS, and the antitumor activity of ONC by investigating whether this cytotoxic enzyme may trigger chemosensitivity of pancreatic adenocarcinoma cells to GEM.

2. Materials and Methods

2.1. Chemicals

Recombinant onconase was produced and purified from *E. coli*, extracted from inclusion bodies, and then refolded as previously described [24]. Chloroquine diphosphate [CQ; *N*4-(7-chloro-4-quinolinyl)-*N*1,*N*1-dimethyl-1,4-pentanediamine], 3-methyladenine (3MA), *N*-acetyl-L-cysteine (NAC), and everolimus (EVE; RAD-001) were obtained from Sigma (Milan, Italy). Gemcitabine (2′,2′-difluoro-2′-deoxycytidine; GEM) was provided by Accord Healthcare (Milan, Italy) and solubilized in sterile water.

2.2. Cell culture

Panc1 and PaCa44 human pancreatic adenocarcinoma cell lines were grown in RPMI 1640 supplemented with 2 mM glutamine

(Life Technologies, Milan, Italy), 10% FBS, and 50 μg/ml gentamicin sulfate (BioWhittaker, Lonza, Bergamo, Italy). Normal primary fibroblasts (PromoCell, PBI, Milan, Italy) and HaCaT non-tumorigenic keratinocytes were grown in DMEM supplemented with 2 mM glutamine (Life Technologies, Milan, Italy), 10% FBS, and 50 μg/ml gentamicin sulfate. All cell types were incubated at 37 °C with 5% CO_2.

2.3. Cell proliferation assay

Cells were seeded in 96-well plates (2.5×10^3 cells/well) and, the day after, at the times indicated in figure legends, they were incubated with ONC and/or various compounds. At the end of the treatments, cells were stained with a crystal violet solution (Sigma, Milan, Italy). The dye was solubilized in PBS containing 1% SDS and photometrically measured ($A_{595\ nm}$) to determine cell growth.

2.4. Apoptosis assay

Cells were seeded in 96-well plates (2.5×10^3 cells/well) and, the day after, treated for 72 h with the various compounds at the indicated concentrations. At the end of the treatment, cells were fixed with 2% paraformaldehyde in PBS at room temperature for 30 min, then washed twice with PBS and stained for 10 min in the dark at room temperature with annexin V/FITC (Bender MedSystem, Milan, Italy) in binding buffer (10 mM HEPES/HCl pH 7.4, 140 mM NaCl, and 2.5 mM $CaCl_2$). Finally, cells were washed with binding buffer solution and fluorescence was measured with a multimode plate reader (λ_{exc} 485 nm and λ_{em} 535 nm) (GENios Pro, Tecan, Milan, Italy). Values were normalized on cell proliferation by crystal violet assay.

2.5. Monodansylcadaverine staining and autophagosome detection

To quantify the induction of autophagy, cells were incubated with monodansylcadaverine (MDC; Sigma, Milan, Italy), a selective fluorescent probe for autophagosome detection. Briefly, cells were seeded in 96-well plates (2.5×10^3 cells/well) and treated with the various compounds indicated in the figure legends. At the end of the treatments, cells were incubated for 15 min in culture medium with 50 μM MDC at 37 °C. After incubation, cells were washed with Hanks buffer (20 mM Hepes pH 7.2, 10 mM glucose, 118 mM NaCl, 4.6 mM KCl, and 1 mM $CaCl_2$) and fluorescence was measured by using a multimode plate reader (λ_{exc} 340 nm and λ_{em} 535 nm) (GENios Pro, Tecan, Milan, Italy). Values were normalized on cell proliferation by crystal violet assay.

2.6. GFP-LC3 translocation and quantitative analyses

Cells were transfected with pEGFP-LC3B plasmid using Lipofectamine 2000 (Life Technologies). After transfection, cells were treated with 100 μg/ml onconase for 72 h prior to fixation. Image acquisition was performed with a Leica fluorescence microscope at 40× magnification. To determine the percentage of cells showing GFP-LC3B puncta, the number of green dots was counted in at least 150 cells from randomly placed positions within each sample. Cells showing more than 10 dots have been considered autophagic cells.

2.7. Acridine orange staining and autolysosome detection

Cells (1.6×10^4) were grown on coverslips and treated with onconase as indicated. To assess nuclear morphology, cells were incubated with Hoechst at RT for 2 min. Cell staining was performed with acridine orange (AO; Molecular Probes/Invitrogen) at a final concentration of 5 μg/ml for a period of 10 min (37 °C, 5% CO_2), according to the protocol indicated by the manufacturer. After washing with PBS three times, images were obtained using a Leica fluorescence microscope at 40× magnification.

To quantify autolysosome formation, cells untreated or treated with onconase were stained with AO following the manufacturer's instructions. Autolysosome formation was performed measuring the red/green fluorescence intensity ratio of AO staining (AO green fluorescence λ_{exc} 485 nm and λ_{em} 535 nm; AO red fluorescence λ_{exc} 430 nm and λ_{em} 590 nm) in a multimode plate reader (GENios Pro, Tecan, Milan, Italy). Values were normalized on cell proliferation by crystal violet assay.

2.8. siRNA transfection and Beclin1 silencing

Exponentially growing cells were seeded at a density of 2.5×10^3 cells/well in 96-well plates for autophagosome assay and at 2.5×10^5 cells/plate in 60 mm cell culture plates for protein extraction. Twenty-four hours later, transfections were carried out with a specific small interfering (si) RNA duplex targeting Beclin1 mRNA (5′-ACAGUG AAUUUAAACGACAGCAGCU-3′ and 5′-AGCUGCUGUCGUUUAAAUUC ACUGU-3′) and with a non-targeting negative control siRNA-CTRL (5′-CAGUCGCGUUUGCGACUGG-3′) purchased by Life Technologies (Monza MB, Italy). Cells were transfected with siRNAs at a final concentration of 50 nM using Lipofectamine 2000 (Life Technologies) for 24 h. At the end of transfection time, the cell medium was changed and cells were treated with onconase for 72 h.

2.9. Transient over-expression of UCP2 and MnSOD

Exponentially growing cells were seeded at a density of 5×10^3 cells/well in 96-well plates. Twenty-four hours later, transfections were carried out with a pCR3.1 expression vector containing the cDNA of human MnSOD (kindly provided by Dr. Akashi, National Institute of Radiological Sciences, Chiba, Japan) and/or with a pCMV expression vector containing the human cDNA of UCP2 (OriGene Technologies, Rockville, MD) using Lipofectamine 2000 (Life Technologies), according to the manufacturer's instructions. Cells transfected with the empty vector were used as a negative control and behaved as the untransfected cells (data not shown). Cells were incubated for 24 h and then treated with onconase for the indicated period.

2.10. Immunoblot analysis

Cells were harvested, washed in phosphate-buffered solution, and re-suspended in RIPA buffer (50 mM Tris–HCl pH 8.0, 150 mM NaCl, 1% Igepal CA-630, 0.5% Na-Doc, 0.1% SDS, 1 mM Na_3VO_4, 1 mM NaF, 2.5 mM EDTA, 1 mM PMSF, and 1× protease inhibitor cocktail). After three freeze/thaw cycles and incubation on ice for 30 min, lysate was centrifuged at 14,000 ×*g* for 10 min at 4 °C, and the supernatant used for Western blotting. Protein concentration was measured with the Bradford protein assay reagent (Pierce, Milan, Italy) using bovine serum albumin as a standard. Protein extracts (50 μg/lane) were electrophoresed through a 12% SDS-polyacrylamide gel and electroblotted onto PVDF membranes (Merck-Millipore, Milan, Italy). Membranes were incubated in blocking solution [5% BSA in TBST (50 mM Tris pH 7.5, 0.9% NaCl, 0.1% Tween 20)] for 1 h at room temperature and probed overnight at 4 °C, at 1:1000 final ratio (where not differently specified) with a rabbit monoclonal anti-LC3 (Cell Signaling, cat. no. 2775), a rabbit polyclonal anti-Beclin1 (GeneTex, cat. no. GTX113039), a goat polyclonal anti-UCP2 (Abnova, cat. no. PAB7242), a mouse monoclonal anti-MnSOD antibody (1:2000; Abcam, cat. no. AB16956), a rabbit monoclonal anti-GAPDH (Cell Signaling, cat. no. 5174S), rabbit monoclonal anti-phospho-Akt Ser473 and anti-Akt (Cell Signaling, cat. no. 4060P and no. 9272S, respectively), a mouse monoclonal anti-phopsho-p70S6K Thr389 (Cell Signaling, cat. no. 9206S), or a rabbit monoclonal anti-p70S6K (Cell Signaling, cat. no. 2708S). Horseradish peroxidase conjugated anti-rabbit or anti-mouse IgGs, 1:8000 in blocking solution (Upstate Biotechnology, Milan, Italy), were used to detect specific proteins. Immunodetection was carried

out by using chemiluminescent substrates (GE-Healthcare, Amersham Pharmacia Biotech, Milan, Italy) and recorded with a HyperfilmECL (GE-Healthcare, Amersham Pharmacia Biotech). ECL results were scanned and the amount of protein bands was quantified using NIH Image J software (http://rsb.info.nih.gov/nih-image/) and normalized to the amount of GAPDH detected in the same sample extract.

2.11. Analysis of ROS

The non-fluorescent diacetylated 2′,7′-dichlorofluorescein (DCF-DA) probe (Sigma), which becomes highly fluorescent upon oxidation, was used to evaluate intracellular ROS production. Cells were plated in 96-well plates (5×10^3 cells/well) and treated with various compounds 24 h later, as indicated in the legends to the figures. Then, cells were incubated with 10 μM DCF-DA for 15 min at 37 °C, and DCF fluorescence was measured (λ_{exc} 485 nm and λ_{em} 535 nm) in a multimode plate reader (GENios Pro, Tecan, Milan, Italy). Values were normalized on cell proliferation by the crystal violet assay. To evaluate mitochondrial superoxide ($O_2^{\bullet -}$) production, cells were incubated at 37 °C for 15 min in a culture medium supplemented with 0.5 μM non-fluorescent MitoSox Red probe (Molecular Probes, Invitrogen). Cells were washed with Hanks buffer (20 mM Hepes pH 7.2, 10 mM glucose, 118 mM NaCl, 4.6 mM KCl, and 1 mM $CaCl_2$) and fluorescence was measured in a multimode plate reader (λ_{exc} 430 nm and λ_{em} 590 nm). The probe is live-cell permeant and is rapidly and selectively targeted to mitochondria where it becomes fluorescent after oxidation by $O_2^{\bullet -}$. The usage of 430 ± 35 nm excitation wavelengths allowed us to selectively detect mitochondrial $O_2^{\bullet -}$ and to strongly reduce the recognition of other oxidants (e.g., –OH, $ONOO^{\cdot -}$). Values were normalized on cell proliferation by the crystal violet assay.

2.12. Drug combination studies

Drug combination studies were performed using the 100 μg/ml:1 μM fixed concentration ratio of ONC:GEM, chosen on the basis of onconase and gemcitabine IC_{50} mean values. Taking into account the drug concentration ratios, the in vitro concentration ranges used were 5 μg/ml → 200 μg/ml for ONC and 50 nM → 2 μM for GEM. Concerning onconase and everolimus combination studies, we used the 10 μg/ml:1 μM (ONC:EVE) fixed concentration ratio. The concentration ranges used were 1 μg/ml → 100 μg/ml for ONC and 0.1 μM → 10 μM for EVE. The combination index (CI) values were calculated by the Chou–Talalay equation, which takes into account both potency (IC_{50}) and shape of the dose–effect curve, taking advantage of the CalcuSyn software (Biosoft, Cambridge, UK). The general equation for the classic isobologram is given by $CI = (D)1/(Dx)1 + (D)2/(Dx)2 + [(D)1 \cdot (D)2]/[(Dx)1 \cdot (Dx)2]$, where (Dx)1 and (Dx)2 in the denominators are the doses (or concentrations) of D1 (drug 1) and D2 (drug 2) alone that induces *x*% growth inhibition, whereas (D)1 and (D)2 in the numerators are the doses of drug 1 and drug 2 that in combination also inhibit *x*% cell growth (i.e., isoeffective). CI < 1, CI = 1, or CI > 1 generally indicate synergistic, additive, or antagonistic effect, respectively. CI/effect curves represent the CI versus the fraction (0 → 1) of cells killed by drug combinations. Throughout all experiments, we obtained a linear correlation coefficient of $r > 0.90$.

2.13. Statistical analysis

ANOVA analysis was performed by GraphPad Prism 5 software. *P* value < 0.05 was indicated as to be statistically significant.

3. Results

3.1. Onconase affects growth of pancreatic adenocarcinoma cells more efficiently than normal cells

To analyze the effect and the associated molecular mechanisms of ONC (Fig. 1A) on pancreatic adenocarcinoma cell growth, we used cancer cell lines strongly resistant to standard chemotherapy, such as Panc1 and PaCa44 [25]. Pancreatic cancer cells were highly sensitive to ONC, with a ~60%–65% cell growth inhibition after treatment with 200 μg/ml of enzyme (Fig. 1B). Intriguingly, HaCaT non-tumorigenic keratinocytes (ONC IC_{50} > 200 μg/ml) and normal primary fibroblasts (ONC IC_{50} > 200 μg/ml) were significantly less affected by ONC than cancer cells (ONC IC_{50} = 22.1 ± 0.6 μg/ml for Panc1 cells and 47.9 ± 0.4 μg/ml for PaCa44 cells) (Table 1 and Fig. 1B). According to cell proliferation results, ONC strongly induced apoptosis in pancreatic cancer cells, while non-tumoral cells were considerably less affected (Fig. 1C).

3.2. Onconase triggers Beclin1-mediated autophagy in cancer cells

To further characterize the biological events regulated by ONC in pancreatic adenocarcinoma cells, we investigated whether autophagy may be a mechanism involved in cell growth inhibition. Western blot analysis of the autophagy-related protein LC3 revealed that ONC strongly induced the expression of LC3-II, which is the phosphoethanolaminated and functionally active form of the autophagosome protein LC3-I (Fig. 2A). Since LC3-II translocation in autophagic vesicle membranes is required for autophagosome formation, we analyzed GFP-LC3 localization by fluorescence microscope before and after ONC treatment. We demonstrate that ONC stimulated the formation of green puncta in the cytoplasm of 67% of Panc1 cancer cells (Table 2), as it is representatively shown in Fig. 2B. This result reveals the formation of intracellular autophagosomes, which, after fusion with lysosomes, constitute acidic vesicular organelles (AVOs) detectable by acridine orange (AO), a nucleic acid dye that accumulates in acidic lysosomes. Indeed, since lysosomal enzymes function optimally over a narrow range of acidic pH values, we subsequently used AO staining to evaluate lysosomal acidification. Under low pH conditions, the dye emits red light when excited by blue light. As shown in Fig. 2C, the AO red fluorescence was greatly induced in ONC-treated cells. To eliminate the possibility that the increase of the red fluorescent signal might be due to AO cell loading enhancement, we calculated the ratio of fluorescent intensity from red and green channels in both untreated and ONC-treated cells. Our measurements confirmed that ONC stimulated lysosomal acidification and autolysosome formation in cancer cells (Fig. 2D). To further explore the autophagy pathway induced by ONC in cancer cells, we performed Western blot analyses of the autophagy-related protein Beclin1, which revealed that ONC induced Beclin1 expression (Fig. 2E). In addition, Beclin1 knockdown by siRNA transfection strongly rescued both ONC-mediated Beclin1 increase (Fig. 2E) and autophagosome formation induced by ONC (Fig. 2F), thus establishing that Beclin1 plays a key role in the ONC-stimulated autophagy pathway.

3.3. Onconase-induced autophagy sustains apoptotic cell death in cancer cells

To investigate the role of autophagy on cancer cell response to ONC, we used autophagy inhibitors, such as chloroquine (CQ) or 3-methyladenine (3MA). We first checked the efficiency of both of these inhibitors to repress ONC-stimulated autophagy (Fig. 3A), without

Table 1
IC_{50} values (± SD) of onconase treatment at 72 h.

Cell lines	Panc1	PaCa44	HaCaT	Fibroblasts
IC_{50} (μg/ml)	22.1 ± 0.6	47.9 ± 0.4	>200	>200

IC_{50} represents the concentration of onconase that is required for 50% cell growth inhibition.

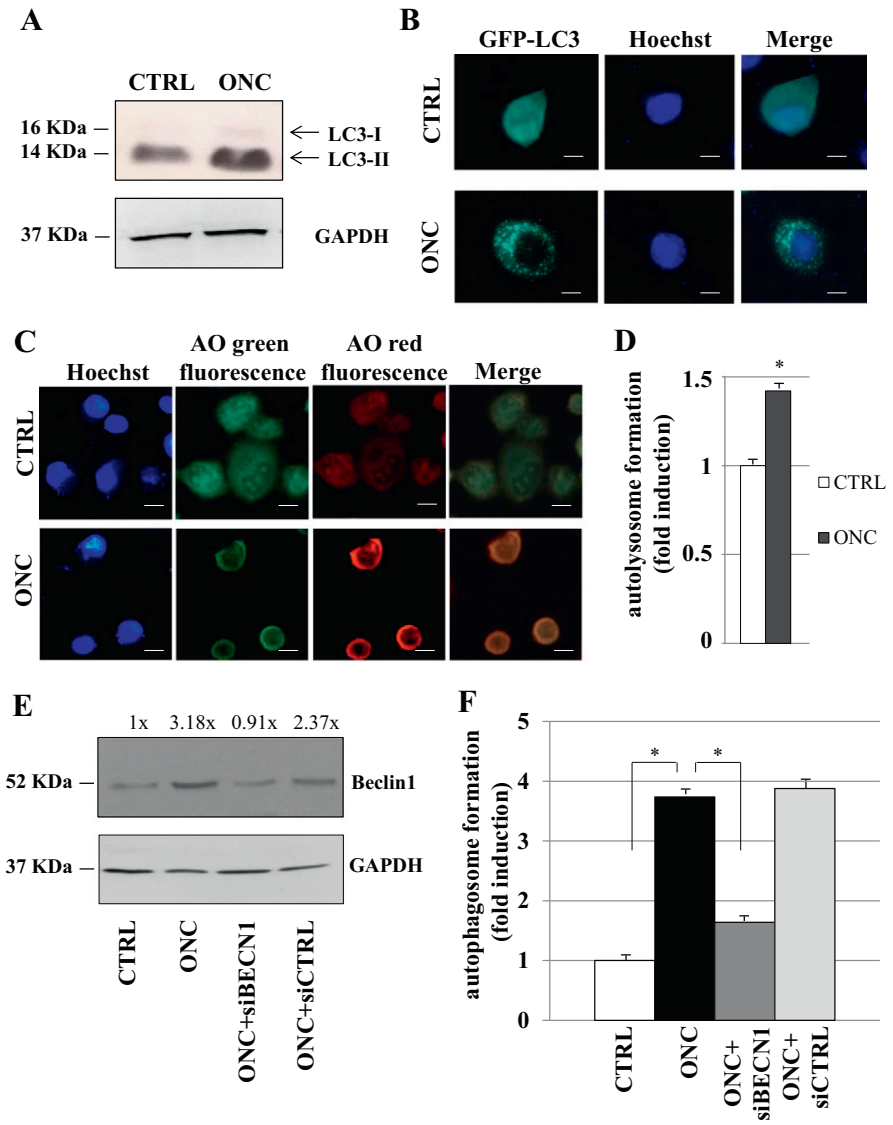

Fig. 2. Onconase induces Beclin1-mediated autophagy. Panc1 cells were treated with 100 μg/ml ONC for 72 h. (A) Western blot of the autophagy-related protein LC3. Cells were seeded in 60-mm diameter culture dishes, incubated overnight, and then treated with ONC. Whole-cell extracts were used for the analysis and GAPDH expression was used as control loading. (B) Accumulation of GFP-LC3B puncta. GFP-LC3B distribution was examined by fluorescence microscopy. Scale bar: 15 μm. (C) Fluorescence microscopy analysis of AO staining in control (CTRL) and ONC-treated cells. Scale bar: 10 μm. (D) Autolysosome formation analyzed by red/green fluorescence intensity ratio quantification of acridine orange (AO) staining after cell treatment with ONC. Values are means (±SD) of three independent biological replicates, each performed using three technical replicates (three wells). Statistical analysis: (*) $p < 0.05$ CTRL versus ONC. (E) Beclin1 expression analyzed by Western blot using whole-cell extracts and GAPDH expression as a control loading. Panc1 cells were seeded in 60-mm diameter culture dishes, incubated overnight, transfected with Beclin1 siRNA (siBECN1) or with negative control siRNA (siCTRL), and/or treated with ONC. The quantification of Beclin1 expression is obtained as described in Materials and Methods and it is reported above the bands, as fold induction relative to control (CTRL). (F) Autophagosome formation assay analyzed by measuring MDC probe incorporation. Panc1 cells were seeded in 96-well plates, incubated overnight, transfected with Beclin1 siRNA or negative control siRNA, and/or treated with ONC Values are means (±SD) of three independent biological replicates, each performed using three technical replicates (three wells). Statistical analysis: (*) $p < 0.05$ ONC versus CTRL or ONC + siBECN1.

triggering cytotoxicity (Fig. 3B) and apoptosis (Fig. 3C) in cancer cells. Importantly, we observed that both CQ or 3MA treatments strongly blocked ONC-mediated apoptosis (Fig. 3D) and significantly reduced ONC-mediated cancer cell growth inhibition (Fig. 3E). Since ONC was also able to stimulate autophagosome formation in normal fibroblasts and HaCaT cells, although at lower levels than in both Panc1 and PaCa44 cancer cell lines (Table 3), we investigated whether this event could play a role in ONC-related growth inhibition of these non-tumoral cells. Interestingly, autophagy inhibitors failed to modify ONC-mediated growth inhibition in normal cell types (Fig. 3F and G). Altogether, these data indicate that autophagy stimulation constitutes a fundamental prerequisite to powerfully inducing ONC-stimulated apoptosis in cancer cells. However, as the recovery by CQ or 3MA of ONC-induced cell growth inhibition is only partial, we cannot exclude that ONC may also stimulate anticancer mechanisms different from apoptosis and autophagy, for instance, for cell cycle arrest and senescence.

Table 2
Percentage of Panc1 cells with GFP-LC3 puncta quantified by analyzing the number of green dots in the cells untreated (CTRL) or treated with 100 μg/ml onconase for 72 h. Data are shown as the mean ± SD of 3 independent experiments.

	Panc1
CTRL	14% ± 4%
ONC	67% ± 6%

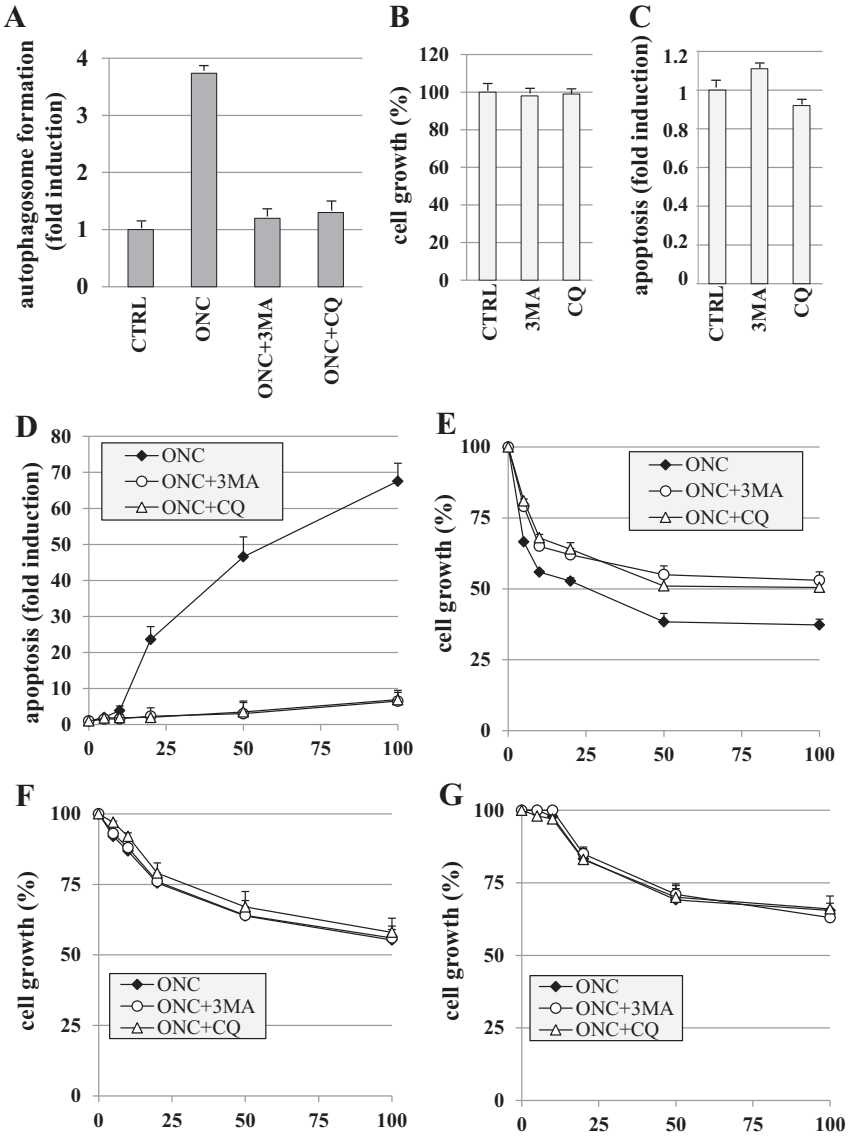

Fig. 3. Role of autophagy induced by ONC. (A) Autophagosome formation assay analyzed measuring MDC probe incorporation. Panc1 cells were seeded in 96-well plates, incubated overnight, and treated with 100 μg/ml ONC, in the absence or presence of 5 μM CQ or 1 mM 3MA for 72 h. Values are means (±SD) of three independent experiments, each performed in triplicate. (B and C) Cell growth and apoptosis determined using crystal violet colorimetric and annexin V/FITC binding assays, respectively. Panc1 cells were seeded in 96-well plates, incubated overnight, and treated with 5 μM CQ or 1 mM 3MA for 72 h. (D and E) Apoptosis and cell growth determined with annexin V/FITC binding and crystal violet colorimetric assays, respectively. Panc1 cells were seeded and treated as described in (A). (F and G) Cell growth of HaCaT cells and fibroblasts, respectively, determined with the crystal violet colorimetric assay. Cells were seeded and treated as described in (A). In all panels, values are means (±SD) of three independent biological replicates, each performed using three technical replicates (three wells).

3.4. Onconase induces mitochondrial superoxide ion production by inhibiting UCP2 and MnSOD expression

To further explore the biological events involved in the regulation of cancer cell proliferation induced by ONC, we investigated whether this enzyme may regulate the redox status of cancer cells. Importantly, Fig. 4A shows that ONC treatment strongly repressed the expression level of both mitochondrial antioxidant uncoupling protein 2 (UCP2) and manganese-dependent superoxide dismutase (MnSOD). In addition, ONC-treated cells showed higher levels of mitochondrial superoxide ion production as compared to untreated cells (Fig. 4B). To functionally evaluate the role of UCP2 and MnSOD inhibition on ONC-mediated ROS increase, we exogenously over-expressed UCP2 or MnSOD proteins (Supplemental Fig. 1A and B). We demonstrate that the exogenous expression of both UCP2 and MnSOD quite totally reduced ONC-mediated cytosolic ROS production (Fig. 4C), revealing that inhibition of both UCP2 and MnSOD is a concerted crucial mechanism lying at the basis of the pro-oxidant effect of ONC in cancer cells. To unravel the biological effect of ROS increase, we analyzed autophagosome formation and cancer cell growth after treatment with ONC and/or the antioxidant molecule NAC. Remarkably, we observed that, in the presence of non-toxic concentrations of NAC, autophagy by ONC was further increased (Fig. 4D). According to the cell death feature of ONC-mediated autophagy stimulation, NAC addition to ONC treatment further decreased cancer cell

Table 3
Autophagosome formation (fold induction ± SD) after treatment with 100 μg/ml onconase for 72 h.

Cell lines	Panc1	PaCa44	HaCaT	Fibroblasts
CTRL	1	1	1	1
ONC	3.73 ± 0.67	4.76 ± 0.53	2.18 ± 0.19	1.48 ± 0.18

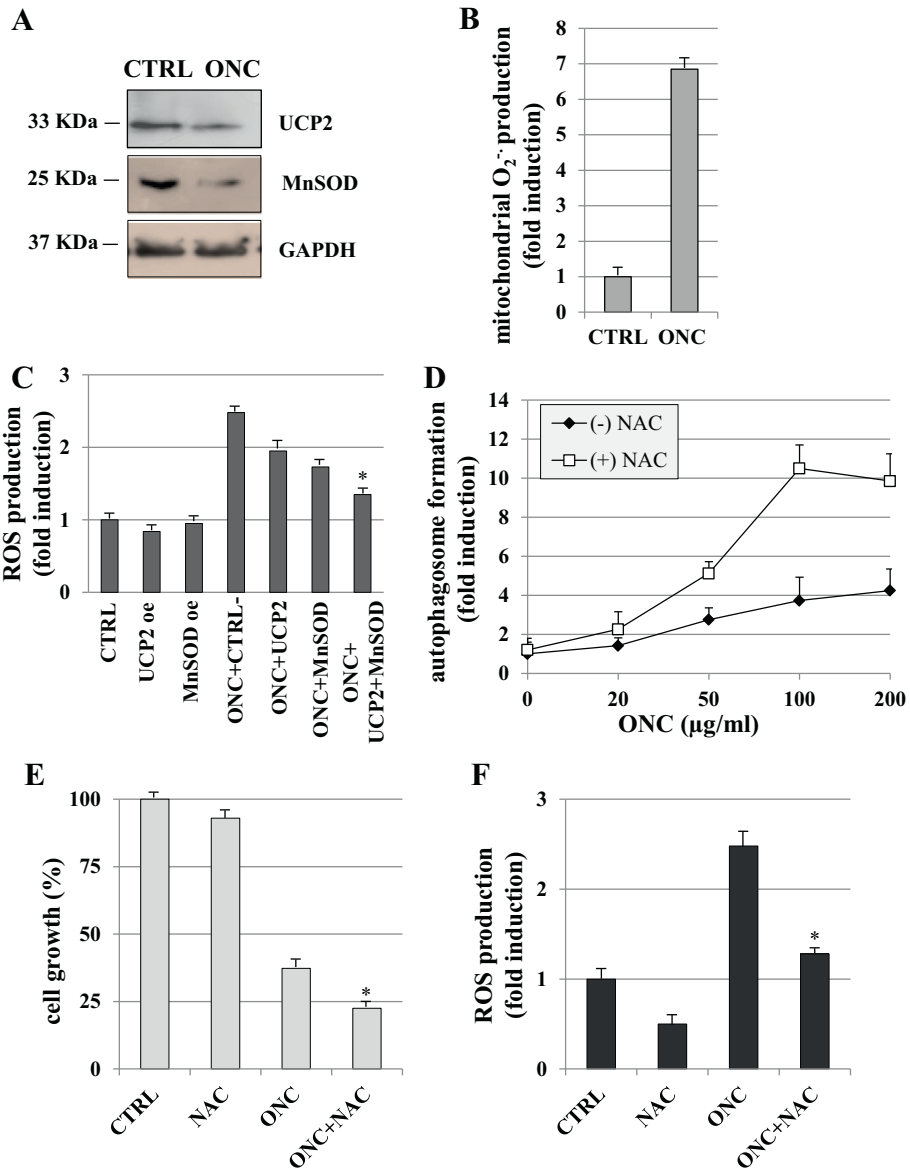

Fig. 4. ROS production stimulated by ONC in Panc1 cells. (A) Western blot of UCP2 and MnSOD. Cells were seeded in 60-mm diameter culture dishes, incubated overnight, and treated with 100 μg/ml ONC for 72 h. Whole-cell extracts were used for the analysis and GAPDH expression was used as control loading. (B) Mitochondrial superoxide production determined with the MitoSox Red probe measured by a multimode plate reader. Cells were seeded in 96-well plates, incubated overnight, and treated with 100 μg/ml ONC for 72 h. (C) DCF fluorescence intensity, corresponding to ROS production level, measured by a multimode plate reader. Cells were seeded in 96-well plates, incubated overnight, and transfected with pCMV-UCP2, pCMV-MnSOD, or empty pCMV vector (CTRL−), in the absence or presence of 100 μg/ml ONC for 72 h. Statistical analysis: (*) $p < 0.05$ ONC + CTRL−, ONC + UCP2, or ONC + MnSOD versus ONC + UCP2 + MnSOD. (D) Autophagosome formation assay analyzed using the MDC probe incorporation. Cells were seeded in 96-well plates, incubated overnight, and treated with increasing concentrations of ONC, in the absence or presence of 10 mM NAC for 72 h. (E and F) Cell growth and ROS production determined with crystal violet colorimetric and DCF fluorescence assays, respectively. Panc1 cells were seeded in 96-well plates, incubated overnight, and treated for 72 h with 100 μg/ml ONC and/or 10 mM NAC. Statistical analysis: (*) $p < 0.05$ ONC versus ONC + NAC. In all panels but (A) the reported values are means (±SD) of three independent biological replicates, each performed using three technical replicates (three wells).

proliferation (Fig. 4E). Finally, to verify the antioxidant property of NAC under the experimental conditions used here, we analyzed ROS production after cell treatment with ONC and/or NAC (Fig. 4F): NAC definitely reduced the amount of ROS produced by ONC alone. Altogether, these data indicate that ROS induction is a mechanism adopted by cancer cells to escape or moderate autophagic cell death induced by ONC.

3.5. Autophagy inhibition by ROS occurs through Akt/mTOR axis stimulation

Since Akt/mTOR axis is a master repressor mechanism of autophagy, we investigated whether autophagy inhibition by ROS occurred through ROS/Akt/mTOR axis stimulation after ONC treatment. We demonstrate that both Akt and p70S6K, the direct target of mTOR commonly used to test its activity, were phosphorylated and activated by ONC and that this stimulation was completely blocked after the addition of NAC. This indicates that ROS induced by ONC stimulated the Akt/mTOR pathway in cancer cells (Fig. 5A). To evaluate the functional role of mTOR stimulation, we analyzed autophagy and cancer cell growth after treatment with ONC and/or everolimus (EVE), a potent mTOR inhibitor. We observed that the combined treatment ONC/EVE strongly enhanced both autophagy (Fig. 5B) and cell growth inhibition (Fig. 5C). To evaluate the synergistic effect of ONC/EVE combination, we analyzed cell growth inhibition curves by using the dedicated specific software CalcuSyn (see Materials and Methods). Dose-dependent analyses performed with different concentrations of ONC and/or EVE showed

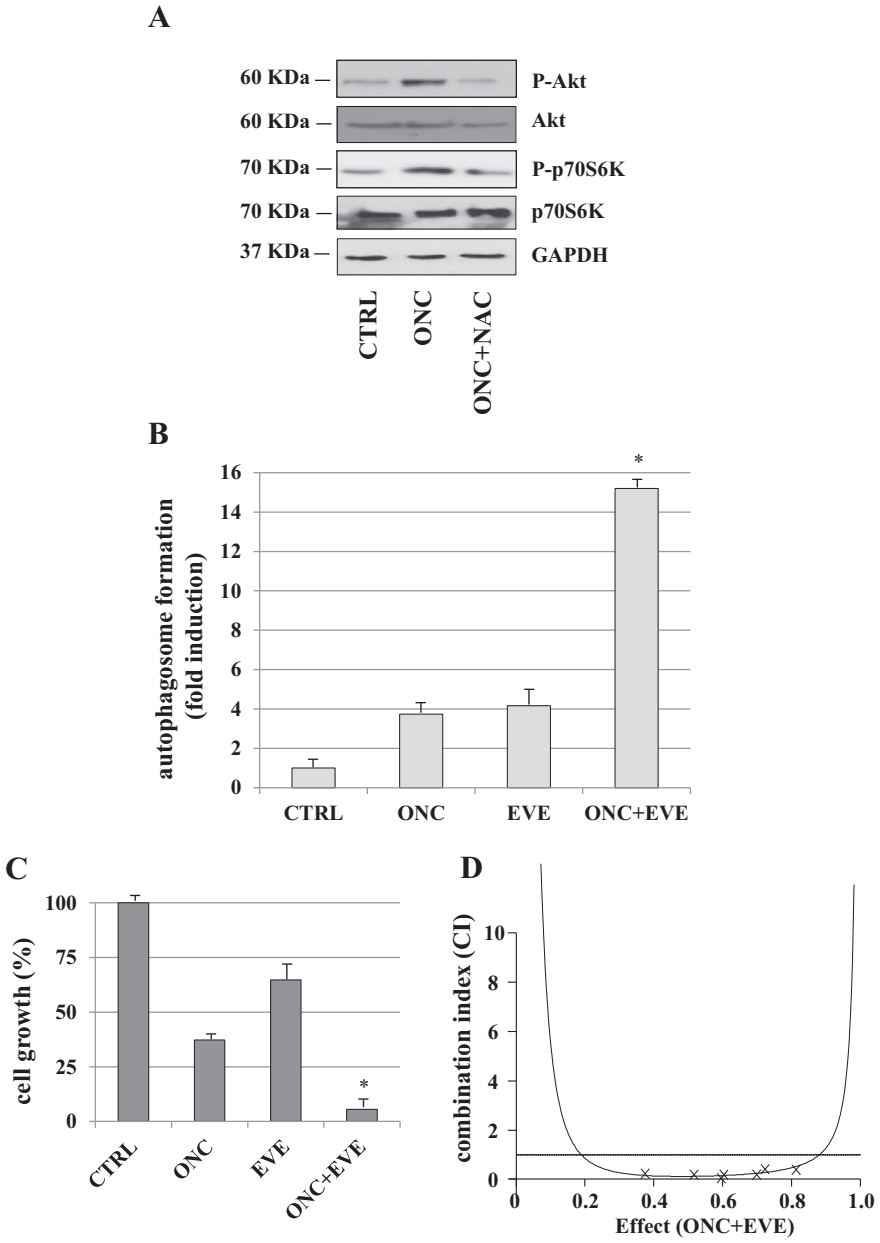

Fig. 5. Onconase triggers ROS/Akt/mTOR axis. (A) Western blot of P-Akt (Ser473), Akt, P-p70S6K (Thr389), and p70S6K Panc1 cells were seeded in 60-mm diameter culture dishes, incubated overnight, and treated with 100 μg/ml ONC in the absence or presence of 10 mM NAC for 72 h. Whole-cell extracts were used for analyses and GAPDH expression as control loading. (B) Autophagosome formation assay analyzed using the MDC probe incorporation. Panc1 cells were seeded in 96-well plates, incubated overnight, and treated with 100 μg/ml ONC and/or 10 μM everolimus for 72 h. (C) Cell growth determined with the crystal violet colorimetric assay. Panc1 cells were treated as described in (B). In both (B) and (C) panels, values are means (±SD) of three independent biological replicates, each performed using three technical replicates (three wells). Statistical analysis: (*) $p < 0.05$ ONC or EVE versus ONC + EVE. (D) CI/fractional effect curve for Panc1 cells treated with a fixed ONC:EVE concentration ratio, as described in Materials and Methods. CIs lying below 1 indicate synergistic conditions.

that the combined setting induces a strong antiproliferative synergism in Panc1 cancer cells, as revealed by the curve of the combination index (CI) values versus the fraction (0 → 1) of cells killed by drug combination (CI_{50} = 0.119; Fig. 5D). Taken together, these data demonstrate that ROS production by ONC reduced autophagic cell death via Akt/mTOR pathway stimulation, which can make cancer cells highly sensitive to mTOR inhibitors.

3.6. Onconase and gemcitabine synergistically inhibit cancer cell growth

Since gemcitabine (GEM) is the standard chemotherapeutic drug used to treat pancreatic adenocarcinoma, and since ROS production [25] and autophagy [14] are molecular mechanisms involved in the response of pancreatic adenocarcinoma cells to GEM, we explored whether the ONC/GEM combined treatment may synergistically induce cancer cell growth inhibition. Fig. 6A shows that ONC treatment in combination with GEM significantly increased Panc1 cell growth inhibition, as compared to single treatments. A similar effect has also been observed in PaCa44 cells (Supplemental Fig. 2A). Dose-dependent analyses performed with different concentrations of ONC and/or GEM showed that the combined setting induced a relevant antiproliferative synergism in Panc1 cancer cells, as revealed by the curve of the combination index (CI) values versus the fraction (0 → 1) of cells killed by drug combination (Fig. 6B). In fact, the CI values lying below 1 are widely distributed in the *x* axis, indicating a synergistic effect occurring at both low and high drug concentrations (Fig. 6B). A similar result has also been observed in PaCa44 cells (Supplemental Fig. 2B). In particular, CI_{25}, CI_{50}, and CI_{75} values for ONC/GEM combination were 0.041, 0.164,

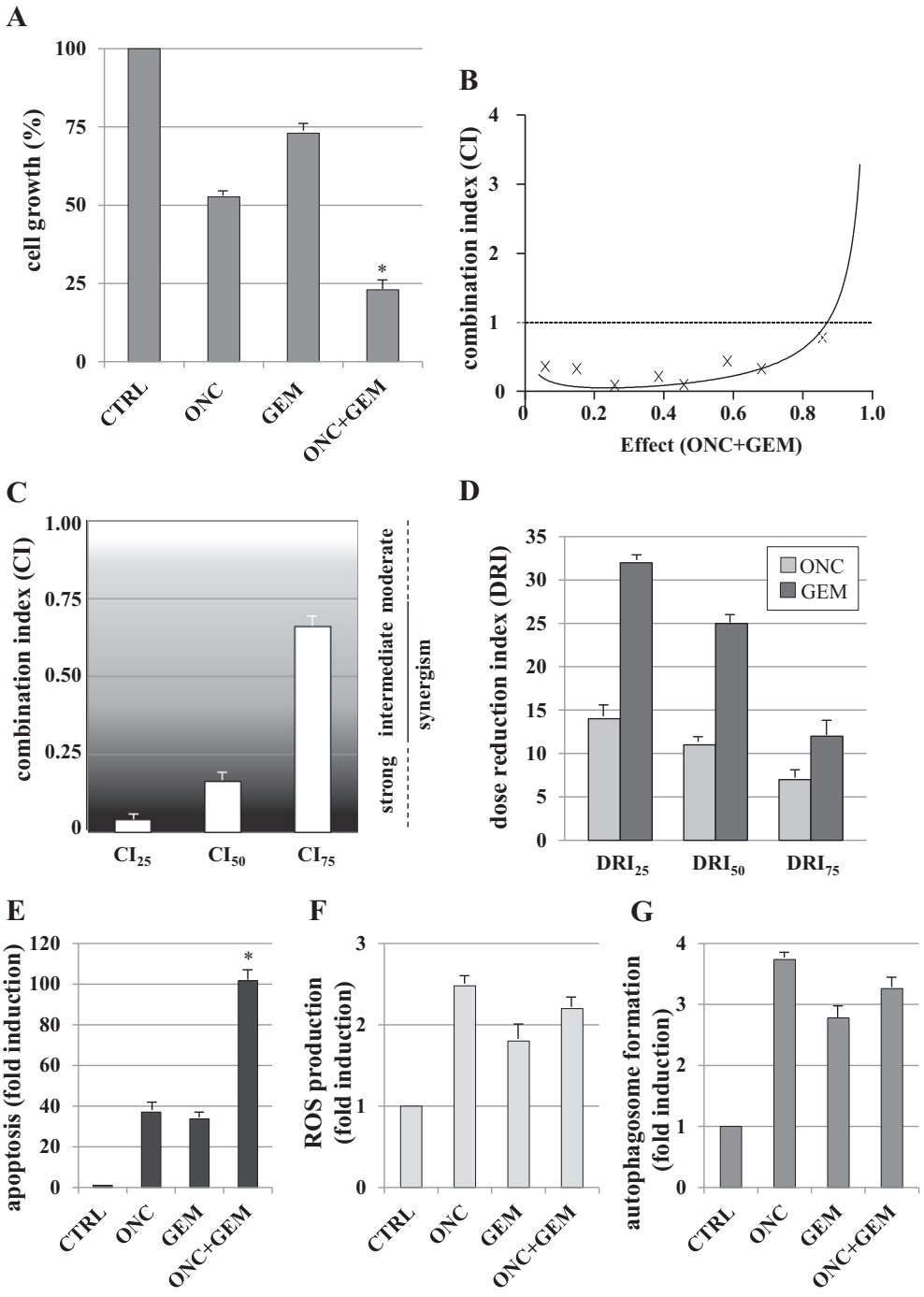

Fig. 6. Onconase and gemcitabine synergistically inhibit cancer cell growth. (A) Cell growth determined with the crystal violet colorimetric assay. Panc1 cells were seeded in 96-well plates, incubated overnight, and treated with 20 μg/ml onconase and/or 200 nM GEM for 72 h. Statistical analysis: (*) $p < 0.05$ ONC or GEM versus ONC + GEM. (B) CI/fractional effect curves for Panc1 cells treated with a fixed ONC:GEM concentration ratio, as described in Materials and Methods. CIs lying below 1 indicate synergistic conditions. (C and D) Combination index (CI) values and dose reduction index (DRI) values calculated for 25%, 50%, or 75% Panc1 cell growth inhibition in the combined treatment ONC + GEM by isobologram analyses performed with the CalcuSyn software. DRI represents the dose reduction folds to obtain 25%, 50%, or 75% cell growth inhibition in a combination setting as compared to each drug alone. (E, F, and G) Apoptosis, ROS production, and autophagosome formation determined with annexin V/FITC binding assay, DCF fluorescence assay, and MDC incorporation assay, respectively. Panc1 cells were seeded in 96-well plates, incubated overnight, and treated with 100 μg/ml ONC and/or 1 μM GEM for 72 h. Statistical analysis in (E): (*) $p < 0.05$ ONC or GEM versus ONC + GEM. In all experiments, values are means (±SD) of three independent biological replicates, each performed using three technical replicates (three wells).

and 0.66, respectively, revealing that the antiproliferative synergism is particularly pronounced at low concentrations of both compounds (Fig. 6C). In addition, we show the reduction folds (dose reduction index; DRI) of drug concentration to obtain 25%, 50%, or 75% cell growth inhibition in combination settings as compared to each drug administered alone (Fig. 6D). According to CIs, Fig. 6D shows values of $DRI_{25} > DRI_{50} > DRI_{75}$ for both compounds, confirming a strong ONC/GEM synergism at low drug concentrations. Furthermore, GEM DRI values are higher than those obtained for ONC, indicating that treatment with this ribonuclease enzyme is able to strongly promote chemosensitization of pancreatic adenocarcinoma cells to standard chemotherapy. Finally, we investigated if apoptosis, autophagy, and ROS production induced by single drug treatments may be further enhanced by ONC/GEM combination. Apoptosis was strongly increased in the combined setting (Fig. 6E), while, surprisingly, ROS production (Fig. 6F) and autophagy were not further stimulated (Fig. 6G).

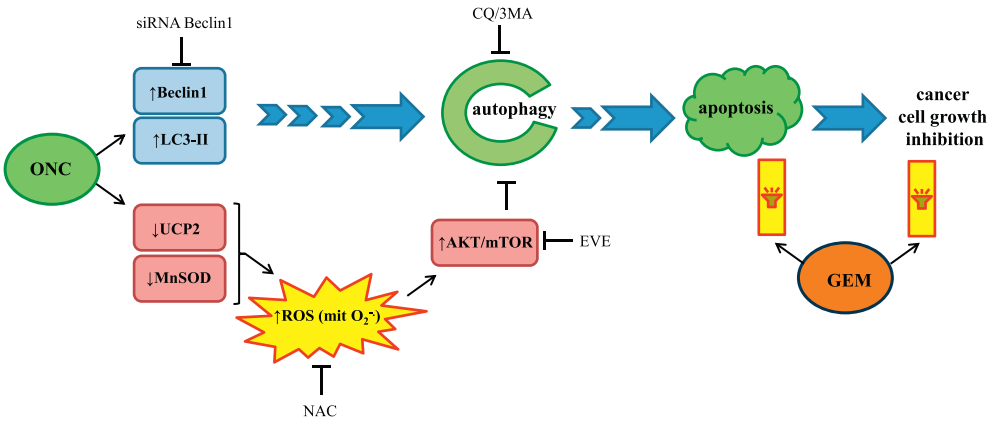

Fig. 7. Model of the molecular mechanisms identified in this study.

Altogether, the results described in the present manuscript, and schematically represented in Fig. 7, indicate that autophagy induced by ONC (mediated by Beclin1 and repressed by ROS/Akt/mTOR axis) is required for ONC-induced apoptosis. Furthermore, autophagy by ONC was further induced by GEM addition promoting their synergistic inhibition of pancreatic adenocarcinoma cell growth.

4. Discussion

In the present manuscript, we demonstrate that ONC strongly affects the proliferation of pancreatic adenocarcinoma cells, while it is significantly less active in normal and non-tumoral cells, as we previously observed for bovine seminal RNase (BS-RNase) [26,27]. This result can be explained with the higher capability of these RNases to interact with the very acidic membrane lipids of cancer cells than with those of normal cells [28–30]. Furthermore, interaction of RNases with cell membrane is augmented upon oligomerization increasing their basic charge density [31–33] or when some key residues are mutated to more basic ones, such as for G38K-BS-RNase [26,28].

Here, we show for the first time that ONC antitumoral activity is mediated by autophagy stimulation. Autophagy is mainly regulated via a group of highly conserved autophagy-related genes (Atg), among which Beclin1 binds to the Class III phosphatidylinositol-3-kinase Vps34, which generates the phosphatidylinositol-3-phosphate (PtdIns-3-P) required for autophagosome formation [34]. Our results, obtained with knockdown assay, reveal that Beclin1 (also called Atg6) is functionally involved in the formation of autophagosomes induced by ONC. According to these data, we previously demonstrated that BS-RNase triggers Beclin1-dependent autophagic cell death in cancer cells providing evidence that high proliferation rates of cancer cells may render them more susceptible to autophagy by BS-RNase treatment [26]. Moreover, autophagy variations in live cells can be monitored by using a GFP-fused LC3 protein (GFP-LC3) analyzing the presence of GFP-LC3 puncta which rapidly increase when autophagy is activated. Accordingly, we demonstrate that ONC treatment strongly increases both LC3-green puncta and autophagosomes in cancer cells. To demonstrate that autophagosome accumulation by ONC is due to autophagy induction, rather than to a block in downstream steps, we observed that ONC increases red/green ratio fluorescence of acridine orange (AO) probe revealing the maturation of autophagy during the final steps. Intriguingly, we demonstrate that the cytotoxic effect of autophagy stimulation induced by ONC is largely due to the shifting of the autophagic process toward proapoptotic signals revealed by the binding of annexin V-FITC to cancer cell membranes. We observed that pharmacological autophagy inhibition by CQ or 3MA strongly represses apoptosis induced by ONC, indicating that autophagy is a fundamental event leading to apoptotic suicide of cancer cells. Indeed, in some circumstances, autophagy can develop as a trigger of apoptosis with a primary response to stress stimuli followed by the promotion of either apoptotic or necrotic final cell death [35].

Since ROS is a major stress stimulator of autophagy and a close relationship between ROS and autophagy exists [36], we investigated whether ONC treatment also modulates ROS production. Notably, in contrast to the unique publication describing an antioxidant effect of ONC in the immortalized line of human T lymphocyte Jurkat cells [37], we demonstrate for the first time that ONC enhances mitochondrial superoxide ion production through the inhibition of the expression of both mitochondrial UCP2 and MnSOD, two of the most important antioxidant systems of mitochondria [38,39]. This suggests a possible differential regulation of the cellular redox status by ONC, which may depend on the cellular model analyzed. However, we surprisingly observed that ROS rescue, by adding the antioxidant NAC, further enhances autophagic cell death by ONC, indicating that ROS acts as compensatory species associated with a mechanism adopted by cancer cells in order to escape or dramatically reduce cytotoxic autophagic stimulation. To explore the mechanism underlying the anti-autophagic role of ONC-induced ROS, we analyzed the activity of mTOR, one of the most powerful enzymatic inhibitors of the autophagic pathway. Our data reveal for the first time that ONC strongly induces the cytosolic Akt/mTOR pathway in a ROS-dependent manner. These results suggest that mitochondrial superoxide generated by ONC through inhibition of UCP2 and MnSOD expression may influence the cytosolic redox status of the cell. Indeed, UCP2 inhibition may enhance the mitochondrial membrane potential, thus causing perturbations of respiratory chain function, electron leakage from electron transport chain (ETC) and higher superoxide production [38]. Since ONC treatment reduces the expression of both UCP2 and MnSOD, the mitochondrial superoxide ion conversion in the membrane-permeable oxidant molecule H_2O_2 is, at least partially, repressed. The stimulation of cytosolic ROS by ONC may thus be explained by observing that superoxide ions produced by electron leakage from complex III of the respiratory chain can be released to both the matrix and the intermembrane space where it can be converted to H_2O_2 by Cu/ZnSOD and released into the cytosol [40,41]. In addition, some evidence indicates that mitochondrial matrix-directed superoxide can be released from the mitochondria through voltage-dependent anion channels (VDAC) increasing cytosolic ROS generation [42]. Our results demonstrate that cytosolic ROS induced by ONC can be quite totally rescued by exogenous expression of UCP2 and MnSOD and indicate that mitochondrial superoxide production can be considered the main source of ROS induced by ONC treatment.

In this study, we show that ROS generated by ONC can induce Akt/mTOR pathway thus promoting chemosensitivity of cancer cells towards mTOR inhibitors that are currently used in clinical trials as anticancer agents [43]. Despite many studies showing that ROS generation can inhibit Akt/mTOR pathway, there is, however, mounting evidence demonstrating that mTOR pathway can be activated by ROS and that

the addition of antioxidants can prevent its stimulation [44–48]. Since mTOR pathway, in addition to promoting protein synthesis, activates specific bioenergetic and anabolic cellular processes that are likely to contribute to human physiology and disease [49], our results can represent a first step in the elucidation of the metabolic reprogramming of cancer cells treated with RNases.

Furthermore, since GEM is the gold standard chemotherapeutic drug in pancreatic adenocarcinoma treatment, we show that ONC association with GEM synergistically inhibits pancreas cancer cell proliferation, without further enhancing autophagy and ROS production but strongly increasing apoptotic cell death. Intriguingly, pancreas cancer cell sensitization to GEM treatment by ONC can determine a reduction of GEM concentration when used in a combination setting, suggesting a lowering of chemotherapy-related side effects in vivo.

5. Conclusions

Overall, the data presented here indicate that ONC strongly inhibits pancreatic adenocarcinoma cell proliferation triggering Beclin1-mediated autophagic cell death and sensitizing cancer cells to apoptotic stimulation by GEM. Inhibition of the mitochondrial antioxidant proteins UCP2 and MnSOD determines a burst of mitochondrial superoxide and of cytosolic ROS responsible for Akt/mTOR pathway activation by ONC, conferring, in turn, cancer cell sensitivity to mTOR inhibitors. Finally, chemosensitization of cancer cells to GEM induced by ONC can be considered as an encouraging therapeutic tool against pancreatic adenocarcinoma.

Supplementary data to this article can be found online at http://dx.doi.org/10.1016/j.bbamcr.2014.12.016.

Acknowledgments

We thank Dr. Marta Menegazzi (University of Verona, Italy) who kindly provided HaCaT non-tumorigenic keratinocytes, and Dr. Eugenio Notomista and Dr. Valeria Cafaro (University of Naples, “Federico II”) who kindly provided plasmid containing ONC cDNA. This work was supported by Ministero dell'Istruzione, dell'Università e della Ricerca (MIUR), Rome, Italy.

References

[1] W. Ardelt, K. Shogen, Z. Darzynkiewicz, Onconase and amphinase, the antitumor ribonucleases from *Rana pipiens* oocytes, Curr. Pharm. Biotechnol. 9 (2008) 215–225.
[2] Z. Darzynkiewicz, S.P. Carter, S.M. Mikulski, W.J. Ardelt, K. Shogen, Cytostatic and cytotoxic effects of Pannon (P-30 Protein), a novel anticancer agent, Cell Tissue Kinet. 21 (1988) 169–182.
[3] W. Ardelt, S.M. Mikulski, K. Shogen, Amino acid sequence of an anti-tumor protein from *Rana pipiens* oocytes and early embryos. Homology to pancreatic ribonucleases, J. Biol. Chem. 266 (1991) 245–251.
[4] E. Boix, Y. Wu, V.M. Vasandani, S.K. Saxena, W. Ardelt, J. Ladner, R.J. Youle, Role of the N terminus in RNase A homologues: differences in catalytic activity, ribonuclease inhibitor interaction and cytotoxicity, J. Mol. Biol. 257 (1996) 992–1007.
[5] T.J. Rutkoski, R.T. Raines, Evasion of ribonuclease inhibitor as a determinant of ribonuclease cytotoxicity, Curr. Pharm. Biotechnol. 9 (2008) 185–189.
[6] M. Naddeo, L. Vitagliano, A. Russo, G. Gotte, G. D'Alessio, S. Sorrentino, Interactions of the cytotoxic RNase A dimers with the cytosolic ribonuclease inhibitor, FEBS Lett. 579 (2005) 2663–2668.
[7] X.M. Wang, Z.Y. Guo, Recombinant expression, different downstream processing of the disulfide-rich anti-tumor peptide Ranpirnase and its effect on the growth of human glioma cell line SHG-44, Biomed. Rep. 1 (2013) 747–750.
[8] P. Smolewski, M. Witkowska, M. Zwolinska, B. Cebula-Obrzut, A. Majchrzak, A. Jeske, Z. Darzynkiewicz, W. Ardelt, B. Ardelt, T. Robak, Cytotoxic activity of the amphibian ribonucleases onconase and r-amphinase on tumor cells from B cell lymphoproliferative disorders, Int. J. Oncol. 45 (2014) 419–425.
[9] W. Ardelt, B. Ardelt, Z. Darzynkiewicz, Ribonucleases as potential modalities in anticancer therapy, Eur. J. Pharmacol. 625 (2009) 181–189.
[10] S.K. Saxena, M. Gravell, Y.N. Wu, S.M. Mikulski, K. Shogen, W. Ardelt, R.J. Youle, Inhibition of HIV-1 production and selective degradation of viral RNA by an amphibian ribonuclease, J. Biol. Chem. 271 (1996) 20783–20788.
[11] A.N. Suhasini, R. Sirdeshmukh, Onconase action on tRNA(Lys3), the primer for HIV-1 reverse transcription, Biochem. Biophys. Res. Commun. 363 (2007) 304–309.
[12] A. Thorburn, D.H. Thamm, D.L. Gustafson, Autophagy and cancer therapy, Mol. Pharmacol. 85 (2014) 830–838.
[13] H. Abeliovich, Regulation of autophagy by amino acid availability in *S. cerevisiae* and mammalian cells, Amino Acids (2014) PMID: 24973972.
[14] M. Donadelli, I. Dando, T. Zaniboni, C. Costanzo, E. Dalla Pozza, M.T. Scupoli, A. Scarpa, S. Zappavigna, M. Marra, A. Abbruzzese, M. Bifulco, M. Caraglia, M. Palmieri, Gemcitabine/cannabinoid combination triggers autophagy in pancreatic cancer cells through a ROS-mediated mechanism, Cell Death Dis. 2 (2011) e152.
[15] I. Dando, C. Fiorini, E.D. Pozza, C. Padroni, C. Costanzo, M. Palmieri, M. Donadelli, UCP2 inhibition triggers ROS-dependent nuclear translocation of GAPDH and autophagic cell death in pancreatic adenocarcinoma cells, Biochim. Biophys. Acta 1833 (2013) 672–679.
[16] T. Ma, J. Zhu, X. Chen, D. Zha, P.C. Singhal, G. Ding, High glucose induces autophagy in podocytes, Exp. Cell Res. 319 (2013) 779–789.
[17] C. Fiorini, M. Menegazzi, C. Padroni, I. Dando, E. Dalla Pozza, A. Gregorelli, C. Costanzo, M. Palmieri, M. Donadelli, Autophagy induced by p53-reactivating molecules protects pancreatic cancer cells from apoptosis, Apoptosis 18 (2013) 337–346.
[18] D. Denton, T. Xu, S. Kumar, Autophagy as a pro-death pathway, Immunol. Cell Biol. (2014). http://dx.doi.org/10.1038/icb.2014.85.
[19] L. Ge, S. Baskaran, R. Schekman, J.H. Hurley, The protein-vesicle network of autophagy, Curr. Opin. Cell Biol. 29C (2014) 18–24.
[20] I. Dando, M. Donadelli, C. Costanzo, E. Dalla Pozza, A. D'Alessandro, L. Zolla, M. Palmieri, Cannabinoids inhibit energetic metabolism and induce AMPK-dependent autophagy in pancreatic cancer cells, Cell Death Dis. 4 (2013) e664.
[21] D. Cecconi, M. Palmieri, M. Donadelli, Proteomics in pancreatic cancer research, Proteomics 11 (2011) 816–828.
[22] M. Herreros-Villanueva, E. Hijona, A. Cosme, L. Bujanda, Adjuvant and neoadjuvant treatment in pancreatic cancer, World J. Gastroenterol. 18 (2012) 1565–1572.
[23] M. Donadelli, E. Dalla Pozza, C. Costanzo, M.T. Scupoli, A. Scarpa, M. Palmieri, Zinc depletion efficiently inhibits pancreatic cancer cell growth by increasing the ratio of antiproliferative/proliferative genes, J. Cell. Biochem. 104 (2008) 202–212.
[24] E. Notomista, V. Cafaro, R. Fusiello, A. Bracale, G. D'Alessio, A. Di Donato, Effective expression and purification of recombinant onconase, an antitumor protein, FEBS Lett. 463 (1999) 211–215.
[25] M. Donadelli, C. Costanzo, S. Beghelli, M.T. Scupoli, M. Dandrea, A. Bonora, P. Piacentini, A. Budillon, M. Caraglia, A. Scarpa, M. Palmieri, Synergistic inhibition of pancreatic adenocarcinoma cell growth by trichostatin A and gemcitabine, Biochim. Biophys. Acta 1773 (2007) 1095–1106.
[26] C. Fiorini, G. Gotte, F. Donnarumma, D. Picone, M. Donadelli, Bovine seminal ribonuclease triggers Beclin1-mediated autophagic cell death in pancreatic cancer cells, Biochim. Biophys. Acta 1843 (2014) 976–984.
[27] G. Gotte, D.V. Laurents, A. Merlino, D. Picone, R. Spadaccini, Structural and functional relationships of natural and artificial dimeric bovine ribonucleases: new scaffolds for potential antitumor drugs, FEBS Lett. 587 (2013) 3601–3608.
[28] G. D'Errico, C. Ercole, M. Lista, E. Pizzo, A. Falanga, S. Galdiero, R. Spadaccini, D. Picone, Enforcing the positive charge of N-termini enhances membrane interaction and antitumor activity of bovine seminal ribonuclease, Biochim. Biophys. Acta 1808 (2011) 3007–3015.
[29] R.F. Turcotte, L.D. Lavis, R.T. Raines, Onconase cytotoxicity relies on the distribution of its positive charge, FEBS J. 276 (2009) 3846–3857.
[30] C. Ercole, R.A. Colamarino, E. Pizzo, F. Fogolari, R. Spadaccini, D. Picone, Comparison of the structural and functional properties of RNase A and BS-RNase: a stepwise mutagenesis approach, Biopolymers 91 (2009) 1009–1017.
[31] M. Libonati, G. Gotte, F. Vottariello, A novel biological actions acquired by ribonuclease through oligomerization, Curr. Pharm. Biotechnol. 9 (2008) 200–209.
[32] G. Gotte, A. Mahmoud Helmy, C. Ercole, R. Spadaccini, D.V. Laurents, M. Donadelli, D. Picone, Double domain swapping in bovine seminal RNase: formation of distinct N- and C-swapped tetramers and multimers with increasing biological activities, PLoS One 7 (2012) e46804.
[33] R. Spadaccini, C. Ercole, G. Graziano, R. Wechselberger, R. Boelens, D. Picone, Mechanism of 3D domain swapping in bovine seminal ribonuclease, FEBS J. 281 (2014) 842–850.
[34] E. Itakura, C. Kishi, K. Inoue, N. Mizushima, Beclin 1 forms two distinct phosphatidylinositol 3-kinase complexes with mammalian Atg14 and UVRAG, Mol. Biol. Cell 19 (2008) 5360–5372.
[35] M.C. Maiuri, E. Zalckvar, A. Kimchi, G. Kroemer, Self-eating and self-killing: crosstalk between autophagy and apoptosis, Nat. Rev. Mol. Cell Biol. 8 (2007) 741–752.
[36] P.J. Vernon, D. Tang, Eat-me: autophagy, phagocytosis, and reactive oxygen species signaling, Antioxid. Redox Signal. 18 (2013) 677–691.
[37] B. Ardelt, G. Juan, P. Burfeind, T. Salomon, J.M. Wu, T.C. Hsieh, X. Li, R. Sperry, P. Pozarowski, K. Shogen, W. Ardelt, Z. Darzynkiewicz, Onconase, an anti-tumor ribonuclease suppresses intracellular oxidative stress, Int. J. Oncol. 31 (2007) 663–669.
[38] M. Donadelli, I. Dando, C. Fiorini, M. Palmieri, UCP2, a mitochondrial protein regulated at multiple levels, Cell. Mol. Life Sci. 71 (2014) 1171–1190.
[39] E. Dalla Pozza, M. Donadelli, C. Costanzo, T. Zaniboni, I. Dando, M. Franchini, S. Arpicco, A. Scarpa, M. Palmieri, Gemcitabine response in pancreatic adenocarcinoma cells is synergistically enhanced by dithiocarbamate derivatives, Free Radic. Biol. Med. 50 (2011) 926–933.
[40] P. Lanciano, B. Khalfaoui-Hassani, N. Selamoglu, A. Ghelli, M. Rugolo, F. Daldal, Molecular mechanisms of superoxide production by complex III: a bacterial versus human mitochondrial comparative case study, Biochim. Biophys. Acta 1827 (2013) 1332–1339.
[41] L. Papa, G. Manfredi, D. Germain, SOD1, an unexpected novel target for cancer therapy, Genes Cancer 5 (2014) 15–21.
[42] M.S. Lustgarten, A. Bhattacharya, F.L. Muller, Y.C. Jang, T. Shimizu, T. Shirasawa, A. Richardson, H. Van Remmen, Complex I generated, mitochondrial matrix-directed superoxide is released from the mitochondria through voltage dependent anion channels, Biochem. Biophys. Res. Commun. 422 (2012) 515–521.

[43] C. Porta, C. Paglino, A. Mosca, Targeting PI3K/Akt/mTOR signaling in cancer, Front. Oncol. 4 (2014) 64.
[44] S. Chen, Q. Ren, J. Zhang, Y. Ye, Z. Zhang, Y. Xu, M. Guo, H. Ji, C. Xu, C. Gu, W. Gao, S. Huang, L. Chen, N-acetyl-L-cysteine protects against cadmium-induced neuronal apoptosis by inhibiting ROS-dependent activation of Akt/mTOR pathway in mouse brain, Neuropathol. Appl. Neurobiol. 40 (6) (2014) 759–777.
[45] J. Yang, T.Z. Li, G.H. Xu, B.B. Luo, Y.X. Chen, T. Zhang, Low-concentration capsaicin promotes colorectal cancer metastasis by triggering ROS production and modulating Akt/mTOR and STAT-3 pathways, Neoplasma 60 (2013) 364–372.
[46] Y.O. Son, P. Pratheeshkumar, L. Wang, X. Wang, J. Fan, D.H. Kim, J.Y. Lee, Z. Zhang, J.C. Lee, X. Shi, Reactive oxygen species mediate Cr(VI)-induced carcinogenesis through PI3K/AKT-dependent activation of GSK-3beta/beta-catenin signaling, Toxicol. Appl. Pharmacol. 271 (2013) 239–248.
[47] R.L. Carpenter, Y. Jiang, Y. Jing, J. He, Y. Rojanasakul, L.Z. Liu, B.H. Jiang, Arsenite induces cell transformation by reactive oxygen species, AKT, ERK1/2, and p70S6K1, Biochem. Biophys. Res. Commun. 414 (2011) 533–538.
[48] L. Chen, B. Xu, L. Liu, Y. Luo, H. Zhou, W. Chen, T. Shen, X. Han, C.D. Kontos, S. Huang, Cadmium induction of reactive oxygen species activates the mTOR pathway, leading to neuronal cell death, Free Radic. Biol. Med. 50 (2011) 624–632.
[49] K. Duvel, J.L. Yecies, S. Menon, P. Raman, A.I. Lipovsky, A.L. Souza, E. Triantafellow, Q. Ma, R. Gorski, S. Cleaver, M.G. Vander Heiden, J.P. MacKeigan, P.M. Finan, C.B. Clish, L.O. Murphy, B.D. Manning, Activation of a metabolic gene regulatory network downstream of mTOR complex 1, Mol. Cell 39 (2010) 171–183.